A preliminary version of this manuscript has been presented at the
5th International Symposium on Solar Sailing, (29 July – 2 August 2019, Aachen, Germany).

Optimal Steering Law of Refractive Sail

Marco Bassetto*, Andrea Caruso, Alessandro A. Quarta, Giovanni Mengali

Department of Civil and Industrial Engineering, University of Pisa, I-56122 Pisa, Italy

Abstract

The interaction between electromagnetic waves and matter is the working principle of a photon-propelled spacecraft, which extracts momentum from the solar radiation to obtain a propulsive acceleration. An example is offered by solar sails, which use a thin membrane to reflect the impinging photons. The solar radiation momentum may actually be transferred to matter by means of various optical phenomena, such as absorption, emission, or refraction. This paper deals with the novel concept of a refractive sail, through which the Sun's light is refracted by crossing a film made of polymeric micro-prisms. The main feature of a refractive sail is to give a large transverse component of thrust even when the sail nominal plane is orthogonal to the Sun-spacecraft line. Starting from the recent literature results, this paper proposes a semi-analytical thrust model that estimates the characteristics of the propulsive acceleration vector as a function of the sail attitude angles. Such a mathematical model is then used to analyze a simplified Earth-Mars and Earth-Venus interplanetary transfer within an optimal framework.

Keywords: Refractive sail, propulsive acceleration model, optimal control law, minimum-time interplanetary transfer

Nomenclature

A	=	sail area, [m^2]
$\boldsymbol{a}$	=	propulsive acceleration vector, [mm/s^2]
a_c	=	characteristic acceleration, [mm/s^2]
a_R	=	radial acceleration, [mm/s^2]
a_T	=	transverse acceleration, [mm/s^2]
$\{c_1, c_2, c_3\}$	=	coefficients of f
$\hat{\boldsymbol{d}}$	=	reference unit vector
$\{\hat{\boldsymbol{e}}_R, \hat{\boldsymbol{e}}_T\}$	=	unit vectors of $\mathcal{T}_S$
f	=	interpolating function
$\mathcal{H}$	=	Hamiltonian function
$\mathcal{H}'$	=	reduced Hamiltonian function
J	=	cost function
$\mathcal{J}$	=	performance index
m	=	spacecraft mass, [kg]
m_p	=	payload mass, [kg]
m_s	=	sail mass, [kg]

*Corresponding author

Email addresses: marco.bassetto@ing.unipi.it (Marco Bassetto), andrea.caruso@ing.unipi.it (Andrea Caruso), a.quarta@ing.unipi.it (Alessandro A. Quarta), g.mengali@ing.unipi.it (Giovanni Mengali)

Published in Advances in Space Research, Vol. 67, No. 9, May 2021, pp. 2855–2864. doi: https://doi.org/10.1016/j.asr.2019.10.033

$\hat{\boldsymbol{n}}$	=	normal unit vector
O	=	Sun's center-of-mass
P_n	=	normal force per unit area at $r = r_\oplus$, [Pa]
p_{n_i}	=	i-th best fit coefficient of P_n
p_R	=	dimensionless radial component of $\boldsymbol{a}$
$\boldsymbol{P}_S$	=	resultant force per unit area at $r = r_\oplus$, [Pa]
P_t	=	tangential force per unit area at $r = r_\oplus$, [Pa]
p_T	=	dimensionless transverse component of $\boldsymbol{a}$
p_{t_i}	=	i-th best fit coefficient of P_t
r	=	Sun-spacecraft distance, [au]
$\hat{\boldsymbol{r}}$	=	Sun-spacecraft unit vector
S	=	spacecraft center-of-mass
t	=	time, [days]
$\hat{\boldsymbol{t}}$	=	tangential unit vector
$\mathcal{T}_B$	=	sail-fixed reference frame
$\mathcal{T}_S$	=	radial-transverse reference frame
$\mathcal{T}_\odot$	=	heliocentric polar reference frame
$\hat{\boldsymbol{v}}$	=	spacecraft velocity unit vector
v_r	=	radial component of spacecraft velocity, [km/s]
v_φ	=	circumferential component of spacecraft velocity, [km/s]
α	=	thrust cone angle, [rad]
α_d	=	angle between $\hat{\boldsymbol{d}}$ and $\hat{\boldsymbol{e}}_R$, [rad]
α_n	=	incidence angle, [rad]
α_λ	=	primer vector angle, [rad]
$\boldsymbol{\lambda}$	=	Lawden's primer vector
$\{\lambda_r, \lambda_\varphi, \lambda_{v_r}, \lambda_{v_\phi}\}$	=	adjoint variables
$\mu_\odot$	=	Sun's gravitational parameter, [km^3/s^2]
τ	=	switching parameter
φ	=	polar angle, [rad]

Subscripts

0	=	initial
f	=	final
$\oplus$	=	calculated at 1 au

Superscripts

$\cdot$	=	time derivative
$\wedge$	=	unit vector
$\star$	=	optimal

1. Introduction

The solar radiation pressure is the physical phenomenon that allows photon-propelled spacecraft to generate a propulsive acceleration. In particular, conventional solar sails [1, 2, 3, 4] exploit a film of reflective material to extract momentum from the impinging photons coming from the Sun. Various missions have already been launched to demonstrate the feasibility of such a fascinating propulsion system, and to evaluate its in-space performance in a real mission scenario. The JAXA's Interplanetary Kite-craft Accelerated by Radiation Of the Sun (IKAROS) has been the first successful interplanetary solar sail demonstration mission [5, 6, 7], which succeeded in deploying a $196\,\mathrm{m}^2$ solar sail in 2010. In the same year, NASA launched the NanoSail-D2 [8], which was a three-unit CubeSat intended to study the deployment mechanism of a $10\,\mathrm{m}^2$ solar sail. The Near-Earth Asteroid Scout (NEA Scout) [9, 10, 11] is another NASA project, scheduled to launch in 2020, whose aim is to fly a six-unit CubeSat towards near-Earth asteroids using a solar sail with an area of $86\,\mathrm{m}^2$. The Planetary Society has recently developed two three-unit CubeSats, the LightSail 1 [12, 13] and LightSail 2 [14]. These CubeSats were launched in 2015 and 2019, respectively, to test the solar sailing in a low-Earth orbit using a $32\,\mathrm{m}^2$ solar sail.

A refractive sail can be considered as an evolution of the solar sail concept since, in principle, it is capable of converting the momentum of the electromagnetic waves through the refraction of the Sun's light across a thin membrane made of polymeric micro-prisms [15]. A good behaviour of a refractive sail requires the diffraction effect to be minimized. This happens when the shortest side of the micro-prisms is at least ten times greater than the longest wavelength [16]. Because the transmissivity of most optical polymers is high in the range $[380,\,1660]\,\mathrm{nm}$ [17, 18], the minimum length of the shortest side of the micro-prisms should be approximately equal to $16.6\,\mu\mathrm{m}$. Note that, however, the thickness of the sail film is also closely related to its manufacturing process and/or to its required mass-to-area ratio. Other current studies [19] have investigated devices that are able to transform an input vortex beam into a quasi-paraxial plane wave, so as to generate a pulling force.

Unlike reflective solar sails, a refractive sail can provide a large transverse thrust when its attitude is nearly Sun-facing, that is, when the sail nominal plane is normal to the Sun-spacecraft line. This interesting feature makes it easier to change the orbit angular momentum, thus allowing many scenarios to be accomplished with a simplified attitude control law, such as the transfer towards rectilinear orbits [20, 21], the generation of logarithmic spiral arcs [22], or the achievement of orbital angular momentum reversal trajectories [23, 24].

In a recent work, [15] have addressed the problem of evaluating the radiation pressure exerted on a refractive sail by means of a ray tracing method [25]. In particular, in their simplified model the assumption is made that the refractive sail has no wrinkles, nor billowing effects, and is perfectly transmissive. With reference to those results, this paper proposes a semi-analytical model, which correlates the propulsive acceleration vector of a refractive sail with its attitude, to look for an analytical approximation of the optimal steering law. The latter results are then used to analyze some transfer trajectories in a preliminary mission design phase. Accordingly, this paper extends the results of [15], who investigated some possible mission applications for a refractive sail, such as the orbit raising from a low-Earth orbit or its attitude control along a single axis normal to the sail nominal plane.

The paper is organized as follows. Section 2 describes the refractive sail propulsive acceleration model starting from the literature results. Section 3 analyzes the sail optimal steering law, which is specialized in Section 4 to a set of simplified minimum-time interplanetary transfers. Section 5 deals with the optimal Earth-Mars and Earth-Venus trajectories, while the last section contains some concluding remarks.

2. Mathematical model

This section introduces a mathematical model aimed at describing the propulsive acceleration vector provided by a refractive sail. To that end, the analysis starts from the results presented by [15], who have recently addressed the problem of determining the thrust of a refractive sail due to the solar radiation pressure.

Consider a two-dimensional radial-transverse reference frame $\mathcal{T}_S(S;\,\hat{\boldsymbol{e}}_R,\,\hat{\boldsymbol{e}}_T)$, centered at the spacecraft center-of-mass S of unit vectors

$$\hat{\boldsymbol{e}}_R \triangleq \hat{\boldsymbol{r}} \quad , \quad \hat{\boldsymbol{e}}_T \triangleq \frac{\hat{\boldsymbol{r}} \times \hat{\boldsymbol{v}}}{\|\hat{\boldsymbol{r}} \times \hat{\boldsymbol{v}}\|} \times \hat{\boldsymbol{r}} \tag{1}$$

where $\hat{\boldsymbol{r}}$ is the Sun-sail unit vector, and $\hat{\boldsymbol{v}}$ is the spacecraft velocity unit vector; see Fig. 1. A sail-fixed two-dimensional reference frame $\mathcal{T}_B(S;\,\hat{\boldsymbol{n}},\,\hat{\boldsymbol{t}})$ is also introduced, in which $\hat{\boldsymbol{n}}$ is perpendicular to the sail nominal plane and points in direction opposite to the Sun, while $\hat{\boldsymbol{t}}$ is tangent to the sail nominal plane and oriented as illustrated in Fig. 1.

Assuming the thrust vector to belong to the spacecraft orbital plane, the sail trajectory is two-dimensional. The sail orientation is therefore univocally determined by its incidence angle α_n, that is, the angle between $\hat{\boldsymbol{n}}$ and $\hat{\boldsymbol{e}}_R$. Note that α_n is positive (or negative) when $\hat{\boldsymbol{n}} \cdot \hat{\boldsymbol{e}}_T > 0$ (or $\hat{\boldsymbol{n}} \cdot \hat{\boldsymbol{e}}_T < 0$). The vector $\boldsymbol{P}_S$ represents the resultant force per unit area due to the solar radiation pressure acting on the refractive sail at a Sun-spacecraft distance $r = r_\oplus \triangleq 1\,\mathrm{au}$, while the angle α between $\boldsymbol{P}_S$ and $\hat{\boldsymbol{e}}_R$ is referred to as thrust cone angle; see Fig. 1.

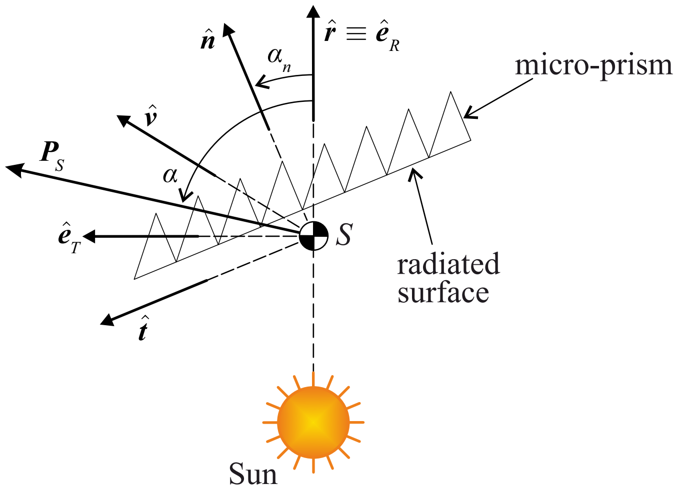

Figure 1: Sketch of reference frames and angles.

The design of a refractive sail requires not only a suitable choice of the geometry of the micro-prisms, but also an accurate selection of their material. In particular, [15] analyze the refractive sail performance through an optimization procedure aimed at maximizing the component of $\boldsymbol{P}_S$ along $\hat{\boldsymbol{t}}$ when $\alpha_n \in [-10, 10]$ deg. To that end, according to [15], polystyrene is the best manufacturing material for a refractive sail. Indeed, polystyrene has the highest dispersion curve (the latter being related to the refractive index) and, therefore, the largest tangential force within a given incidence angle range. The numerical results are reported with dotted lines in Figs. 2(a) and 2(b), in which P_t and P_n are the components of $\boldsymbol{P}_S$ along $\hat{\boldsymbol{t}}$ and $\hat{\boldsymbol{n}}$, respectively, or

$$P_t \triangleq \boldsymbol{P}_S \cdot \hat{\boldsymbol{t}} \quad , \quad P_n \triangleq \boldsymbol{P}_S \cdot \hat{\boldsymbol{n}} \tag{2}$$

Analytical approximations for both P_t and P_n are here proposed in order to obtain a direct correlation between the sail attitude and the components of $\boldsymbol{P}_S$ in the radial-transverse reference frame. To that end, two six-order polynomial interpolations have been used, that is

$$P_t \simeq \sum_{i=0}^{6} p_{t_i}\, \alpha_n^i \quad , \quad P_n \simeq \sum_{i=0}^{6} p_{n_i}\, \alpha_n^i \tag{3}$$

The best fit coefficients p_{t_i} and p_{n_i} are reported in Tab. 1, with α_n measured in radians, while P_t and P_n are given in pascal. A comparison between the polynomial approximations (solid lines) of Eqs. (3) and the

i	p_{t_i}	p_{n_i}
0	1.544×10^{-6}	8.661×10^{-7}
1	-1.235×10^{-6}	-2.294×10^{-6}
2	-7.211×10^{-6}	6.225×10^{-6}
3	4.498×10^{-5}	-8.179×10^{-6}
4	4.749×10^{-4}	-8.317×10^{-5}
5	-2.263×10^{-4}	-4.034×10^{-4}
6	-1.239×10^{-2}	4.264×10^{-3}

Table 1: Best fit coefficients for P_t and P_n; see Eqs. (3) where α_n is in radians, while $\{P_t, P_n\}$ are in pascal.

literature results (dotted lines) is shown in Fig. 2.

In order to evaluate the components of $\boldsymbol{P}_S$ in the radial-transverse reference frame, consider the projec-

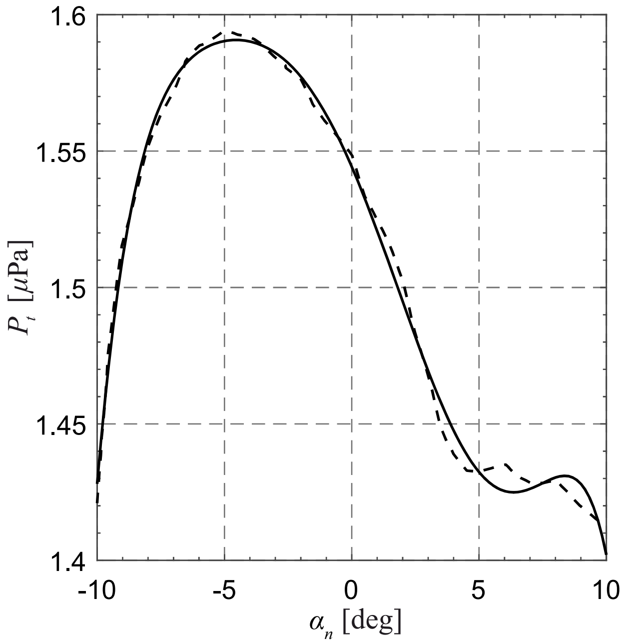

(a) Tangential component.

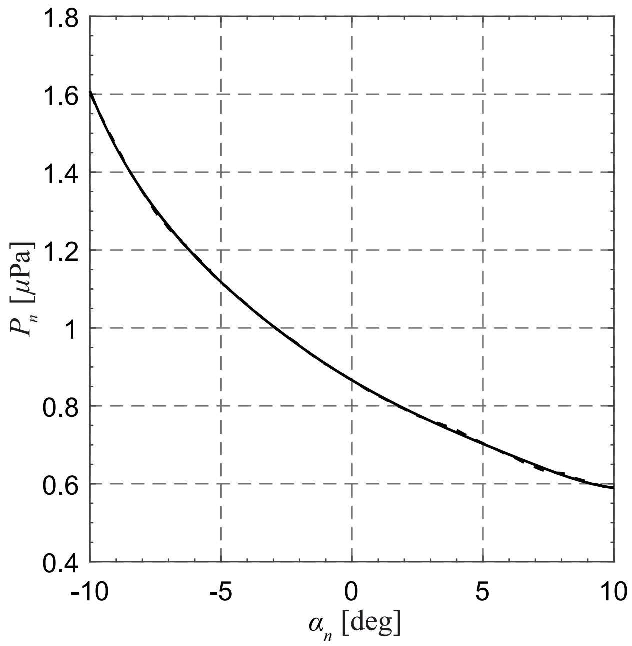

(b) Normal component.

Figure 2: Resultant force per unit area acting on the refractive sail as a function of α_n at 1 au from the Sun. Data from [15] (dotted lines) and polynomial interpolations (solid lines).

tions of $\hat{\boldsymbol{n}}$ and $\hat{\boldsymbol{t}}$ onto $\mathcal{T}_S$, that is

$$\hat{\boldsymbol{n}} = \cos\alpha_n\, \hat{\boldsymbol{e}}_R + \sin\alpha_n\, \hat{\boldsymbol{e}}_T \tag{4}$$

$$\hat{\boldsymbol{t}} = -\sin\alpha_n\, \hat{\boldsymbol{e}}_R + \cos\alpha_n\, \hat{\boldsymbol{e}}_T \tag{5}$$

from which, bearing in mind Eq. (2), the expression of $\boldsymbol{P}_S$ becomes

$$\boldsymbol{P}_S = P_\oplus \left(p_R \, \hat{\boldsymbol{e}}_R + p_T \, \hat{\boldsymbol{e}}_T \right) \tag{6}$$

where $P_\oplus \simeq 4.5391 \, \mu\text{Pa}$ is the solar radiation pressure at the Sun-sail reference distance $r_\oplus$, while

$$p_R \triangleq \left(P_n \, \cos\alpha_n - P_t \, \sin\alpha_n \right) / P_\oplus \tag{7}$$

$$p_T \triangleq \left(P_n \, \sin\alpha_n + P_t \, \cos\alpha_n \right) / P_\oplus \tag{8}$$

are the dimensionless components of $\boldsymbol{P}_S$ in $\mathcal{T}_S$; see Fig. 3. Finally, Fig. 4 shows the thrust cone angle α,

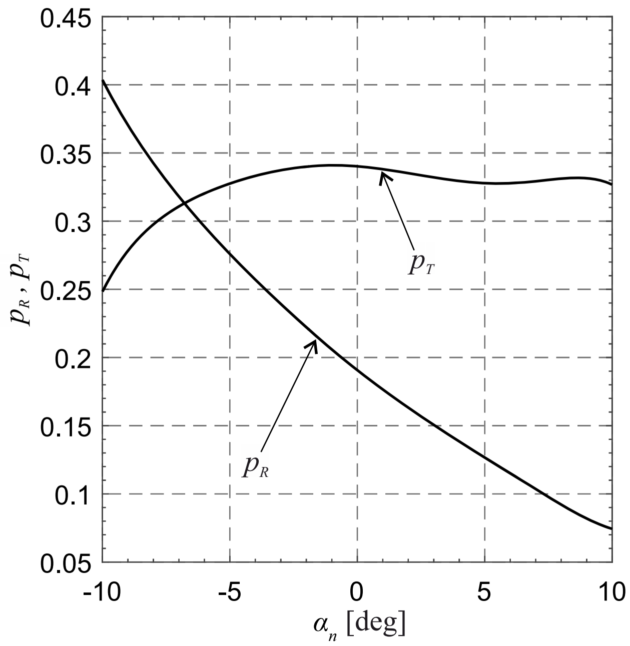

Figure 3: Dimensionless components of $\boldsymbol{P}_S$ in $\mathcal{T}_S$.

defined as

$$\alpha \triangleq \arctan\left(\frac{p_T}{p_R}\right) \tag{9}$$

and the resultant force magnitude per unit area P_S, given by

$$P_S \triangleq \|\boldsymbol{P}_S\| = P_\oplus \sqrt{p_R^2 + p_T^2} \tag{10}$$

as a function of α_n.

Note that p_T is nearly constant with α_n, while p_R is a monotonic decreasing function of the incidence angle. Moreover, a negative transverse component of $\boldsymbol{P}_S$ can be theoretically obtained with a 180 deg rotation of the sail nominal plane about the Sun-spacecraft line. Such a rotation may be accomplished using power-consuming actuators, such as reaction wheels or thrusters. However, [15] show that the refractive sail itself can be used as an attitude control system when the incidence angle is nearly zero and, as such, a rotation about the local radial direction is equivalent to a simple yaw maneuver. In that case, a control torque can be generated through the activation/deactivation of the outer edge of the sail, which, to that end, is divided into several portions as is schematically illustrated in Fig. 5. In particular, polymer dispersed liquid crystal (PDLC) films [26] allow the transmissivity of the refractive sail to be switched from transparent to opaque (or vice versa) by means of an electrostatic field. Therefore, a control torque along the axis normal to the sail may be generated by individually modifying the transmissivity of the refractive portions of the control surface.

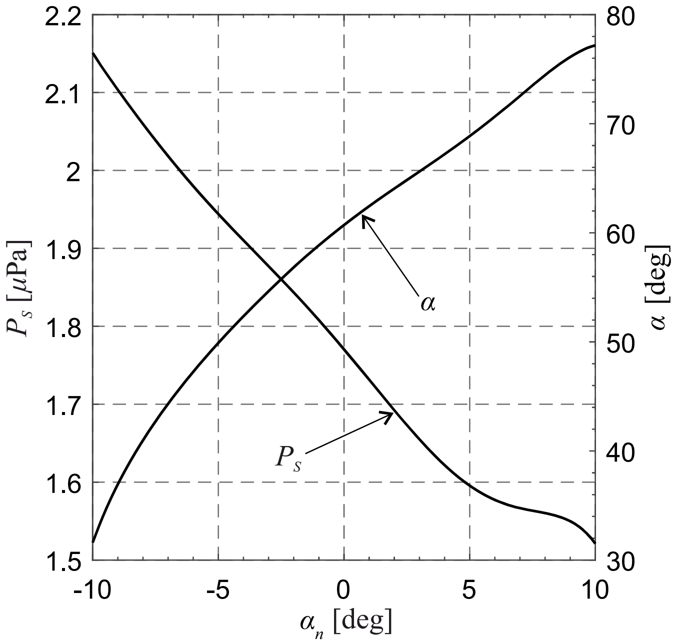

Figure 4: Resultant force magnitude per unit area P_S and thrust cone angle α as a function of α_n.

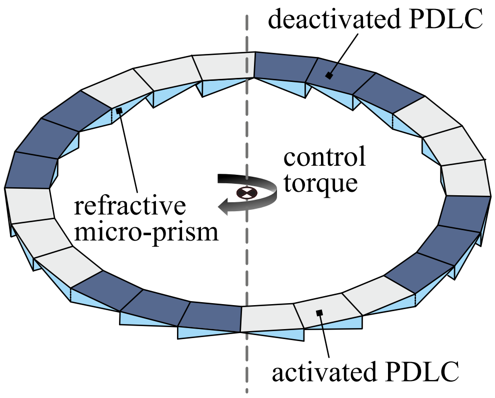

Figure 5: Conceptual scheme of yaw control with PDLC, adapted from [15].

2.1. Refractive sail propulsive acceleration vector

Because the solar radiation pressure scales as the inverse square distance from the Sun, the propulsive acceleration vector $\boldsymbol{a}$ may be written as

$$\boldsymbol{a} = a_R\, \hat{\boldsymbol{e}}_R + a_T\, \hat{\boldsymbol{e}}_T \tag{11}$$

where

$$a_R \triangleq \frac{P_\oplus\, A}{m} \left(\frac{r_\oplus}{r}\right)^2 p_R \quad , \quad a_T \triangleq \tau\, \frac{P_\oplus\, A}{m} \left(\frac{r_\oplus}{r}\right)^2 p_T \tag{12}$$

are the radial and transverse components of the propulsive acceleration vector $\boldsymbol{a}$, respectively. In Eq. (12), p_R and p_T are given by Eqs. (7) and (8), $\tau = \{-1;\, 1\}$ is the switching parameter, which models the possibility of changing the sign of a_T, A is sail area, and $m = (m_s + m_p)$ is the total mass, where m_s and m_p are the sail and payload mass, respectively. Note that

$$\frac{m_p}{A} = \frac{m}{A} - \frac{m_s}{A} \geq 0 \tag{13}$$

where, according to [15], $m_s/A \simeq 0.0105\,\mathrm{kg/m^2}$, a value consistent with that obtained by a conventional solar sail such as IKAROS in which $m_s/A \simeq 0.01\,\mathrm{kg/m^2}$. For the sake of completeness, the values of A, m, and m/A of some solar sail-based spacecraft are reported in Tab. 2.

Mission	A [m^2]	m [kg]	m/A [kg/m^2]
IKAROS	196	315	1.6071
NanoSail D2	10	4	0.4
NEA Scout	86	14	0.1628
LightSail 1/2	32	4.5	0.1406

Table 2: Sail area, total mass, and ratio m/A of the main solar sail-based spacecraft.

The approximate expression of the propulsive acceleration given by Eq. (11) is used in the next section to obtain an analytical form of the sail optimal steering law.

3. Optimal steering law

The analysis of the optimal steering law starts from the evaluation of the pair $\{\alpha_n^\star, \tau^\star\}$ that maximizes the projection of the propulsive acceleration vector $\boldsymbol{a}$ along a given direction, which may be described by an assigned unit vector $\hat{\boldsymbol{d}}$, defined as

$$\hat{\boldsymbol{d}} \triangleq \cos\alpha_d\,\hat{\boldsymbol{e}}_R + \sin\alpha_d\,\hat{\boldsymbol{e}}_T \tag{14}$$

where $\alpha_d \in [0,\, 2\pi)$ rad is the angle between $\hat{\boldsymbol{d}}$ and $\hat{\boldsymbol{e}}_R$; see Fig. (6).

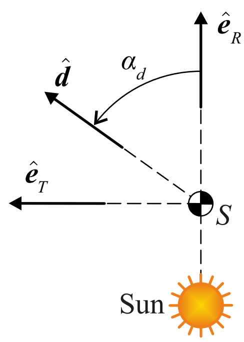

Figure 6: Sketch of unit vector $\hat{\boldsymbol{d}}$.

The solution to this problem is a necessary step for evaluating the minimum flight time necessary to reach a given target orbit with an indirect approach [27, 28, 29], or for determining the optimal thrust vector in a locally optimal framework, that is, when the performance index to minimize is a function of the time derivative of the spacecraft osculating orbital elements [30, 31].

The problem of maximizing the projection of $\boldsymbol{a}$ along $\hat{\boldsymbol{d}}$ amounts to that of maximizing the scalar product between $\boldsymbol{a}$ and $\hat{\boldsymbol{d}}$. To that end, consider the dimensionless cost function $J = J(\alpha_n,\, \tau,\, \alpha_d)$, defined as

$$J \triangleq \frac{\boldsymbol{a}\cdot\hat{\boldsymbol{d}}}{\dfrac{P_\oplus\, A}{m}\left(\dfrac{r_\oplus}{r}\right)^2} = p_R\,\cos\alpha_d + \tau\, p_T\,\sin\alpha_d \tag{15}$$

where p_R and p_T are obtained from Fig. 3 or by Eqs. (7)-(8).

Because $p_T > 0$ for all α_n, see Fig. 3, the cost function J is maximized when

$$\tau = \tau^\star \triangleq \text{sign}\{\sin \alpha_d\} \tag{16}$$

Accordingly, Eq. (15) may be rewritten as

$$J = p_R \cos \alpha_d + p_T \, |\sin \alpha_d| \tag{17}$$

which implies that $J = J(\alpha_n, \alpha_d)$. For a given value of α_d, the optimal incidence angle $\alpha_n = \alpha_n^\star$ that maximizes the cost function J may be easily obtained numerically, for example with a golden section search-based routine. The optimal incidence angle is reported in Fig. 7 as a function of α_d using the results of [15] to estimate the thrust vector characteristics.

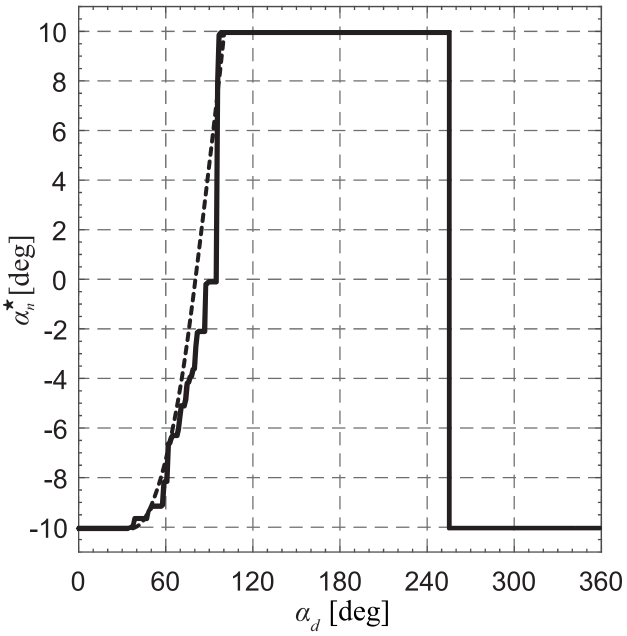

Figure 7: Optimal incidence angle $\alpha_n = \alpha_n^\star$ as a function of α_d (solid line) and its approximation as per Eq. (18) (dotted line).

Note that the function $\alpha_n^\star = \alpha_n^\star(\alpha_d)$ may be accurately approximated by

$$\alpha_n^\star = \begin{cases} -10 \text{ deg} & \text{if} \quad \alpha_d \in [0,\, 34) \text{ deg} \\ f(\alpha_d) & \text{if} \quad \alpha_d \in [34,\, 97) \text{ deg} \\ 10 \text{ deg} & \text{if} \quad \alpha_d \in [97,\, 256) \text{ deg} \\ -10 \text{ deg} & \text{if} \quad \alpha_d \in [256,\, 360) \text{ deg} \end{cases} \tag{18}$$

where $f = f(\alpha_d)$ is an auxiliary function defined as

$$f(\alpha_d) \triangleq c_1 \, \alpha_d^2 + c_2 \, \alpha_d + c_3 \tag{19}$$

with $c_1 \simeq 0.0050 \, \text{deg}^{-1}$, $c_2 \simeq -0.3427$, and $c_3 \simeq -4.1749 \, \text{deg}$. Figure 7 also compares the exact and approximate values of the optimal incidence angle.

To summarize, for a given value of α_d (that is, for a given direction $\hat{\boldsymbol{d}}$), the optimal values of τ and α_n that maximize the projection of $\boldsymbol{a}$ along $\hat{\boldsymbol{d}}$ are given by Eq. (16) and (18), respectively.

4. Trajectory optimization

Consider now a refractive sail-based spacecraft and introduce a heliocentric polar reference frame $\mathcal{T}_\odot(O;\, r,\, \varphi)$, whose origin coincides with the Sun's center-of-mass O, in which r is the Sun-spacecraft distance, and φ is the polar angle measured from the Sun-spacecraft direction at the initial time $t = t_0 \triangleq 0$; see Fig. 8.

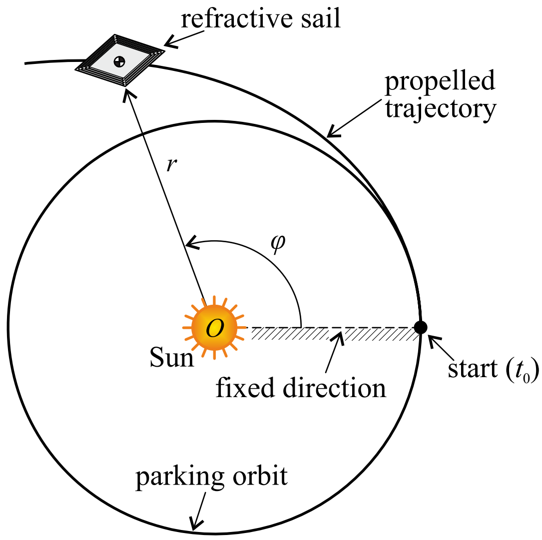

Figure 8: Sketch of the heliocentric polar reference frame.

The two-dimensional spacecraft equations of motion in $\mathcal{T}_\odot$ are

$$\dot{r} = v_r \tag{20}$$

$$\dot{\varphi} = \frac{v_\varphi}{r} \tag{21}$$

$$\dot{v}_r = -\frac{\mu_\odot}{r^2} + \frac{v_\varphi^2}{r} + a_R \tag{22}$$

$$\dot{v}_\varphi = -\frac{v_r\, v_\varphi}{r} + a_T \tag{23}$$

where $\mu_\odot$ is the Sun's gravitational parameter, v_r (or v_φ) is the radial (or circumferential) component of the spacecraft inertial velocity, while a_R and a_T are obtained from Eqs. (12) and Eqs. (7)-(8). Note that the incidence angle $\alpha_n \in [-10,\, 10]$ deg and the switching parameter $\tau \in \{-1;\, 1\}$ are the two control variables.

The refractive sail trajectory is analyzed in an optimal framework by minimizing the flight time t_f required to transfer the spacecraft from a circular parking orbit of radius r_0 to a coplanar target orbit of given radius $r_f \neq r_0$. The optimization problem consists in finding the optimal control laws $\alpha_n^\star = \alpha_n^\star(t)$ and $\tau^\star = \tau^\star(t)$ that maximize the performance index

$$\mathcal{J} \triangleq -t_f \tag{24}$$

The optimal trajectory is obtained with an indirect approach. The Hamiltonian function is [32]

$$\mathcal{H} = \lambda_r\, v_r + \lambda_\varphi\, \frac{v_\varphi}{r} + \lambda_{v_r} \left(-\frac{\mu_\odot}{r^2} + \frac{v_\varphi^2}{r} + a_R\right) + \lambda_{v_\varphi} \left(-\frac{v_r\, v_\varphi}{r} + a_T\right) \tag{25}$$

where $\{\lambda_r,\, \lambda_\varphi,\, \lambda_{v_r},\, \lambda_{v_\varphi}\}$ are the adjoint variables associated with the spacecraft states $\{r,\, \varphi,\, v_r,\, v_\varphi\}$. The time derivatives of the adjoint variables are given by the Euler-Lagrange equations, viz.

$$\dot{\lambda}_r = -\frac{\partial \mathcal{H}}{\partial r} = \lambda_\varphi \frac{v_\varphi}{r^2} - \lambda_{v_r} \left(\frac{2\,\mu}{r^3} - \frac{v_\varphi^2}{r^2} - \frac{2\,a_R}{r} \right) - \lambda_{v_\varphi} \left(\frac{v_r\, v_\varphi}{r^2} - \frac{2\,a_T}{r} \right) \tag{26}$$

$$\dot{\lambda}_\varphi = -\frac{\partial \mathcal{H}}{\partial \varphi} = 0 \tag{27}$$

$$\dot{\lambda}_{v_r} = -\frac{\partial \mathcal{H}}{\partial v_r} = -\lambda_r + \lambda_{v_\varphi} \frac{v_\varphi}{r} \tag{28}$$

$$\dot{\lambda}_{v_\varphi} = -\frac{\partial \mathcal{H}}{\partial v_\varphi} = -\frac{\lambda_\varphi}{r} - 2\,\lambda_{v_r} \frac{v_\varphi}{r} + \lambda_{v_\varphi} \frac{v_r}{r} \tag{29}$$

From Eq. (27), it turns out that λ_φ is a constant of motion. The set of differential equations (20)–(23) and (26)–(29) are completed by four conditions at the initial time t_0

$$r(t_0) = r_0 \quad , \quad \varphi(t_0) = v_r(t_0) = 0 \quad , \quad v_\varphi(t_0) = \sqrt{\frac{\mu_\odot}{r_0}} \tag{30}$$

and by four conditions at the (unknown) final time t_f

$$r(t_f) = r_f \quad , \quad v_r(t_f) = \lambda_\varphi(t_f) = 0 \quad , \quad v_\varphi(t_f) = \sqrt{\frac{\mu_\odot}{r_f}} \tag{31}$$

Finally, the two-point boundary value problem is completed by the transversality condition [32]

$$\mathcal{H}(t_f) = 1 \tag{32}$$

From the Pontryagin's maximum principle, the optimal control law maximizes the Hamiltonian function at any time. This amounts to maximizing the portion of $\mathcal{H}$ that explicitly depends on the controls, that is

$$\mathcal{H}' \triangleq \lambda_{v_r}\, a_R + \lambda_{v_\varphi}\, a_T \tag{33}$$

The latter may also be rewritten as

$$\mathcal{H}' = \lambda\, (a_R\, \cos\alpha_\lambda + a_T\, \sin\alpha_\lambda) \tag{34}$$

where $\lambda \triangleq \sqrt{\lambda_{v_r}^2 + \lambda_{v_\varphi}^2}$ is the magnitude of the primer vector $\boldsymbol{\lambda} \triangleq [\lambda_{v_r}\ \ \lambda_{v_\varphi}]^{\mathrm{T}}$ [33], while

$$\cos\alpha_\lambda \triangleq \frac{\lambda_{v_r}}{\sqrt{\lambda_{v_r}^2 + \lambda_{v_\varphi}^2}} \quad , \quad \sin\alpha_\lambda \triangleq \frac{\lambda_{v_\varphi}}{\sqrt{\lambda_{v_r}^2 + \lambda_{v_\varphi}^2}} \tag{35}$$

where $\alpha_\lambda \in [0,\, 2\pi)\,\text{rad}$ is the primer vector angle. Bearing in mind Eq. (12), the reduced Hamiltonian function $\mathcal{H}'$ becomes

$$\mathcal{H}' = \lambda\, \frac{P_\oplus\, A}{m} \left(\frac{r_\oplus}{r}\right)^2 (p_R\, \cos\alpha_\lambda + \tau\, p_T\, \sin\alpha_\lambda) \tag{36}$$

A comparison between Eqs. (15) and (36) demonstrates that the optimal control law is given by Eqs. (16) and (18) by formally substituting α_d with α_λ.

5. Case study

The proposed thrust model and optimization procedure are used to analyze the minimum-time heliocentric orbit raising (or lowering) of a refractive sail-based spacecraft. For exemplary purposes, consider a vehicle that initially covers a circular parking orbit of radius $r_0 = r_\oplus$. Such a situation corresponds to a sail deployment on a parabolic escape orbit relative to the Earth, and with the assumption that the Earth's orbital eccentricity is zero.

The circular target orbit is a heliocentric coplanar orbit of radius $r_f = 1.523\,\mathrm{au}$ (or $r_f = 0.723\,\mathrm{au}$). This mission scenario is consistent with an ephemeris-free Earth-Mars (or Earth-Venus) interplanetary transfer, in which both the eccentricity and the inclination of the planet orbits are neglected. The aim of this section is indeed to evaluate the performance of a refractive sail in a heliocentric mission context. The solutions are parameterized with the reference acceleration $P_\oplus\, A/m$, which is considered as an input parameter during the optimization process.

Assume first a refractive sail characterized by $P_\oplus\, A/m = 1\,\mathrm{mm/s^2}$, which corresponds to a high performance propulsion system with $m/A \simeq 0.0045\,\mathrm{kg/m^2}$ (such a performance is not yet obtainable with the current technology level since, from Eq. (13), $m/A \geq m_s/A = 0.0105\,\mathrm{kg/m^2}$). Note that, in this case, the maximum obtainable propulsive acceleration when $r = r_\oplus$ is about $0.478\,\mathrm{mm/s^2}$. With such a performance level, the minimum flight time for an Earth-Mars mission case is $t_f \simeq 400\,\mathrm{days}$, while an Earth-Venus transfer requires about 202 days. The corresponding transfer trajectories are shown in Figs. 9(a) and 9(b). In both cases, the achievement of the final target orbit occurs in less than one revolution around the Sun.

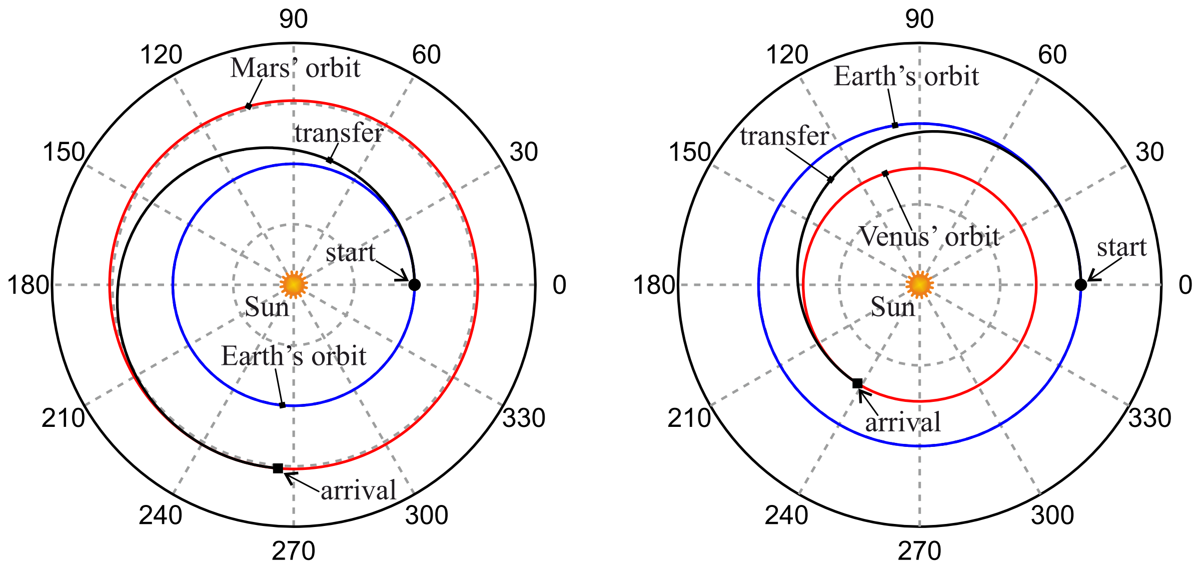

(a) Earth-Mars transfer.

(b) Earth-Venus transfer.

Figure 9: Optimal transfer trajectories for $P_\oplus\, A/m = 1\ \mathrm{mm/s^2}$.

The situation is more involved when the value of the reference propulsive acceleration is sufficiently small. Consider, for example, $P_\oplus\, A/m = 0.1\,\mathrm{mm/s^2}$, that is, $m/A \simeq 0.0454\,\mathrm{kg/m^2}$, which corresponds to a feasible case with $m_p/A \simeq 0.0349\,\mathrm{kg/m^2} > 0$. In this case, the maximum obtainable propulsive acceleration when $r = r_\oplus$ is about $0.047\,\mathrm{mm/s^2}$. Both the Earth-Mars and the Earth-Venus optimal transfers require about 6 complete revolutions around the Sun, as is shown in Figs. 10(a) and 10(b). In that cases, the flight times are about 3090 and 1778 days, respectively.

The optimal steering law is plotted in Fig. 9 for the two case studies with $P_\oplus\, A/m = 1\,\mathrm{mm/s^2}$. Note that, when the orbit angular momentum has to be increased (or reduced), the value of $\tau^\star$ is equal to 1 (or -1) for most of the transfer. In particular, the grey area shown in Fig. 11(a) (or 11(b)) corresponds to the time interval within which $\tau^\star = -1$ (or $\tau^\star = 1$). Therefore, in both cases, the optimal control law entails only two rotation maneuvers of the refractive sail around the radial direction.

The problem of evaluating the optimal transfer trajectory may be addressed in a parametric way by looking for the minimum transfer time when the reference propulsive acceleration $P_\oplus\, A/m$ ranges within the interval $[0.1,\, 1]\,\mathrm{mm/s^2}$, that is, when considering a medium-high performance refractive sail. The results are shown in Figs. 12 and 13 for the Earth-Mars and the Earth-Venus transfers, respectively. As expected, the total flight time increases when the reference propulsive acceleration reduces, with a rapid variation when

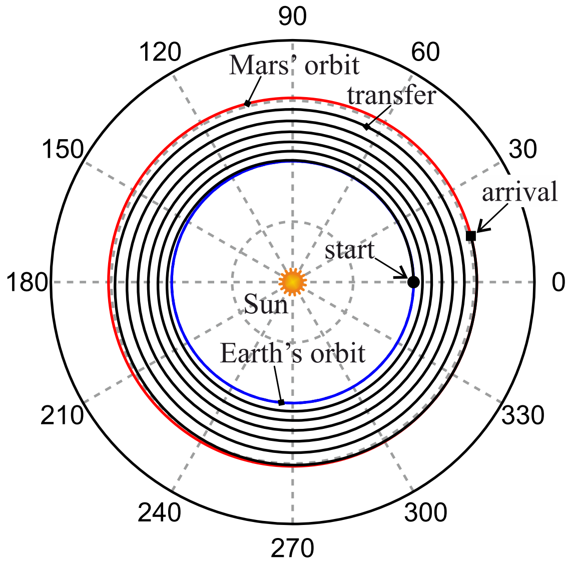

(a) Earth-Mars transfer.

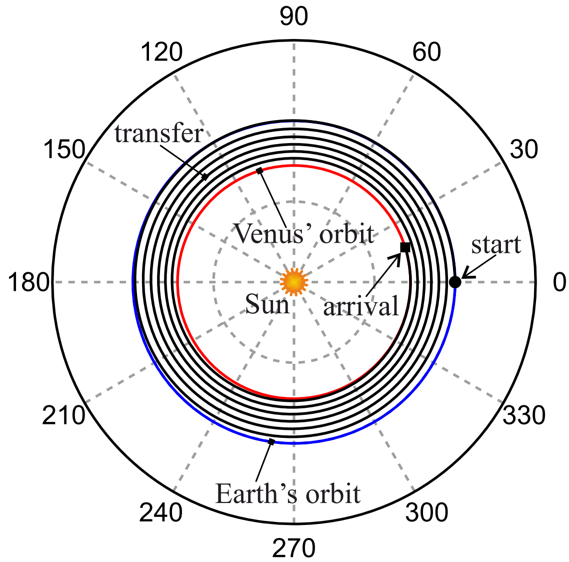

(b) Earth-Venus transfer.

Figure 10: Optimal transfer trajectories for $P_{\oplus}\, A/m = 0.1$ mm/s^2.

$P_{\oplus}\, A/m$ becomes less than $0.3\,\mathrm{mm/s^2}$.

It is interesting to compare the minimum flight times with those attainable with a conventional reflective sail. Such a comparison has been performed assuming the same maximum acceleration at the reference distance of 1 au. Therefore, the circle-to-circle Earth-Mars and Earth-Venus optimal transfers have also been investigated using a solar sail with characteristic acceleration $a_c = \{0.478,\, 0.047\}\,\mathrm{mm/s^2}$, and using an optical force model [1] in the simulations. The results, which are reported in Tab. 3, show that the use of a refractive sail always entails a decrease of the total flight time. In particular, for the Earth-Mars optimal transfers, the flight times decrease more than 44%, whereas there is (at least) a 30% reduction of mission length for the Earth-Venus minimum-time trajectories.

	Reflective sail		Refractive sail	
$\max\{a\}$ at 1 au $[\mathrm{mm/s^2}]$	0.478	0.047	0.478	0.047
Earth-Mars [days]	720	6163	400	3090
Earth-Venus [days]	291	2706	202	1778

Table 3: Comparison between minimum Earth-Mars and Earth-Venus transfer times.

6. Conclusions

This paper has dealt with the novel concept of a refractive sail-based spacecraft. A thrust model has been provided starting from the recent literature results. The main feature of such a propulsion system is the large transverse component of the propulsive acceleration that may be obtained when the sail nominal plane is orthogonal to the Sun-spacecraft line. Two-dimensional circle-to-circle interplanetary transfers have been studied in an optimal framework by means of an indirect approach, and minimum-time trajectories corresponding to ephemeris-free Earth-Mars and Earth-Venus transfers have been analyzed. For example, using a high performance refractive sail, the optimal transfers towards Mars and Venus require about 400 days and 202 days, respectively. These numbers show that such a propulsion system represents an alternative solution to reflective solar sails in case of minimum-time problems.

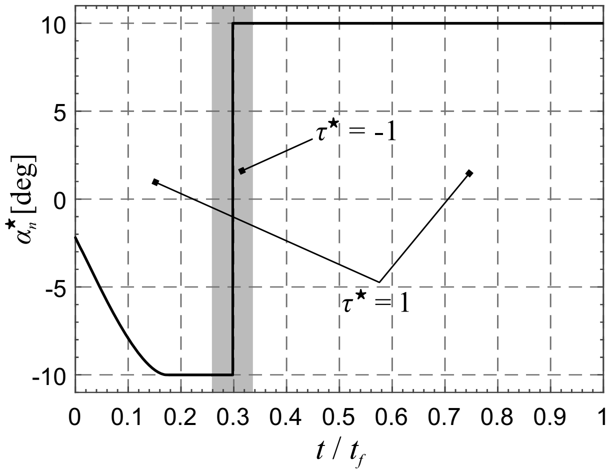

(a) Earth-Mars transfer.

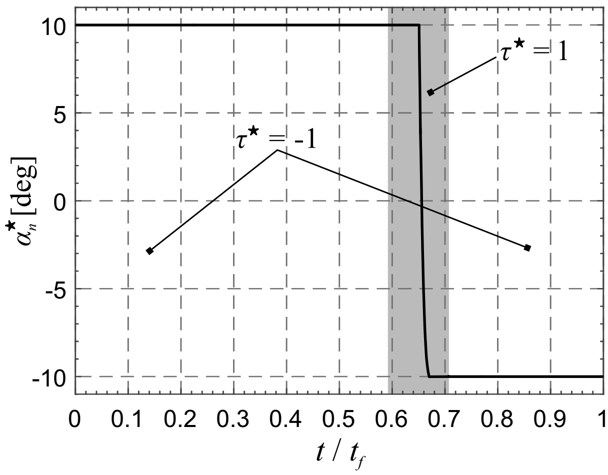

(b) Earth-Venus transfer.

Figure 11: Optimal control law for $P_\oplus\, A/m = 1$ mm/s^2.

The refractive sail may be a promising option for many other missions, such as the design of heliocentric escape trajectories (useful for the study of the Heliosheath and the interstellar medium), or the maintenance of displaced non-Keplerian orbits (advantageous for observing the planetary polar regions). Future investigations will concentrate on the analysis of those challenging scenarios.

References

[1] C. R. McInnes, Solar Sailing: Technology, Dynamics and Mission Applications, Springer-Praxis Series in Space Science and Technology, Springer-Verlag, Berlin, 2004, Ch. 6, pp. 229–270, ISBN: 978-3540210627.

[2] B. Fu, E. Sperber, F. Eke, Solar sail technology - A state of the art review, Progress in Aerospace Sciences 86 (2016) 1–19, doi: 10.1016/j.paerosci.2016.07.001.

[3] D. Zola, C. Circi, G. Vulpetti, S. Scaglione, Photon momentum change of quasi-smooth solar sails, Journal of the Optical Society of America A: Optics and Image Science, and Vision 35 (8) (2018) 1261–1271, doi: 10.1364/JOSAA.35.001261.

[4] S. Gong, M. Macdonald, Review on solar sail technology, Astrodynamics 3 (2) (2019) 93–125, doi: 10.1007/s42064-019-0038-x.

[5] R. Funase, O. Mori, Y. Tsuda, Y. Shirasawa, T. Saiki, Y. Mimasu, J. Kawaguchi, Attitude control of IKAROS solar sail spacecraft and its flight results, in: 61st International Astronautical Congress, Prague, Czech Republic, 2010, paper IAC-10.C1.4.3.

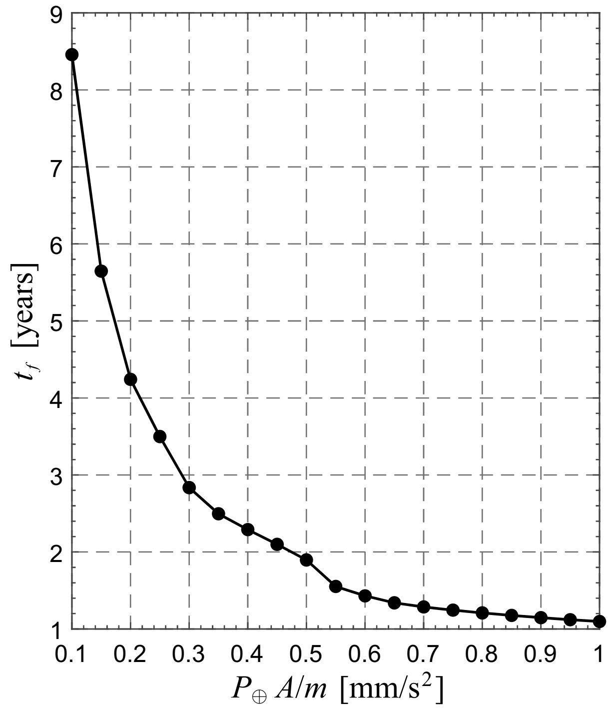

Figure 12: Minimum Earth-Mars flight time as a function of $P_\oplus\, A/m \in [0.1,\, 1]$ mm/s^2.

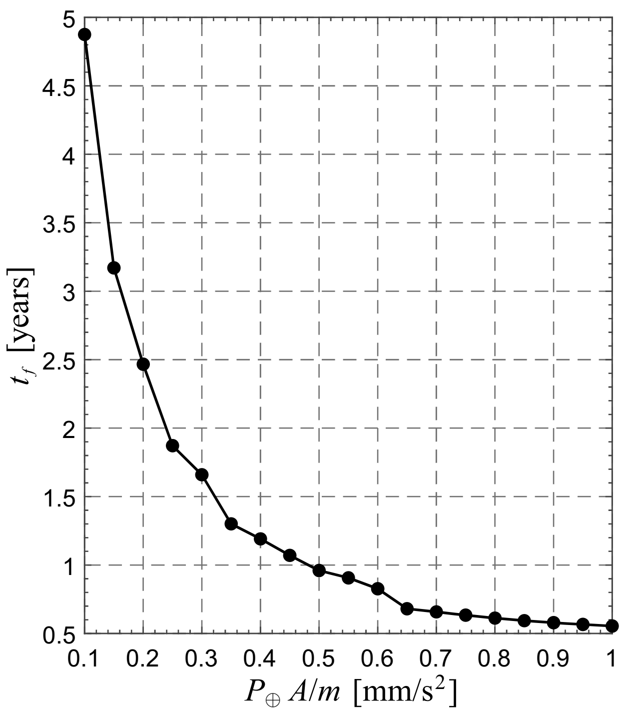

Figure 13: Minimum Earth-Venus flight time as a function of $P_\oplus\, A/m \in [0.1,\, 1]$ mm/s^2.

[6] R. Funase, J. Kawaguchi, O. Mori, H. Sawada, Y. Tsuda, IKAROS, a solar sail demonstrator and its application to Trojan asteroid exploration, in: 53rd AIAA/ASME/ASCE/AHS/ASC Structural Dynamics and Materials Conference, Honolulu

(HI), USA, 2012, AIAA Paper 2012-1748.
[7] Y. Tsuda, O. Mori, R. Funase, H. Sawada, T. Yamamoto, T. Saiki, T. Endo, K. Yonekura, H. Hoshino, J. Kawaguchi, Achievement of IKAROS - Japanese deep space solar sail demonstration mission, Acta Astronautica 82 (2) (2013) 183–188, doi: 10.1016/j.actaastro.2012.03.032.
[8] L. Johnson, M. Whorton, A. Heaton, R. Pinson, G. Laue, C. Adams, NanoSail-D2: A solar sail demonstration mission, Acta Astronautica 68 (5-6) (2011) 571–575, doi: 10.1016/j.actaastro.2010.02.008.
[9] L. McNutt, L. Johnson, P. Kahn, J. Castillo-Rogez, A. Frick, Near-Earth Asteroid (NEA) Scout, in: AIAA SPACE 2014 Conference and Exposition, San Diego (CA), USA, 2014, AIAA Paper 2014-4435.
[10] L. Johnson, J. Castillo-Rogez, J. Dervan, L. McNutt, Near-Earth Asteroid (NEA) Scout, in: The 4th International Symposium on Solar Sailing, Kyoto, Japan, 2017, paper 17002.
[11] J. Pezent, R. Sood, A. Heaton, Near-Earth Asteroid (NEA) Scout solar sail contingency trajectory design and analysis, in: Space Flight Mechanics Meeting, Kissimmee (FL), USA, 2018, AIAA Paper 2018-0199.
[12] T. Svitek, L. Friedman, W. Nye, C. Biddy, M. Nehrenz, Voyage continues - Lightsail-1 mission by the Planetary Society, in: 61st International Astronautical Congress, Prague, Czech Republic, 2010, paper IAC-10.D1.1.10.
[13] B. Betts, B. Nye, J. Vaughn, E. Greeson, R. Chute, D. Spencer, R. Ridenoure, R. Munakata, S. Wong, A. Diaz, D. Stetson, J. Foley, J. Bellardo, B. Plante, Lightsail 1 mission results and public outreach strategies, in: The 4th International Symposium on Solar Sailing, Kyoto, Japan, 2017, paper 17093.
[14] B. Betts, D. A. Spencer, B. Nye, R. Munakata, J. Bellardo, S. Wong, A. Diaz, R. Ridenoure, B. Plante, J. Foley, J. Vaughn, Lightsail 2: Controlled solar sailing using a CubeSat, in: The 4th International Symposium on Solar Sailing, Kyoto, Japan, 2017, paper 17053.
[15] S. Firuzi, S. Gong, Refractive sail and its applications in solar sailing, Aerospace Science and Technology 77 (2018) 362–372, doi: 10.1016/j.ast.2018.03.016.
[16] A. Ashkin, Forces of a single-beam gradient laser trap on a dielectric sphere in the ray optics regime, Biophysical Journal 61 (2) (1992) 569–582, doi: 10.1016/S0006-3495(92)81860-X.
[17] N. G. Sultanova, S. N. Kasarova, I. D. Nikolov, Investigation of optical properties of thin polymer films, Journal of Physics: Conference Series 356 (1) (2012) Article number 012049, doi: 10.1088/1742-6596/356/1/012049.
[18] N. G. Sultanova, S. N. Kasarova, I. D. Nikolov, Characterization of optical properties of optical polymers, Optical and Quantum Electronics 45 (3) (2013) 221–232, doi: 10.1007/s11082-012-9616-6.
[19] S. Firuzi, S. Gong, Long-range optical pulling force device based on vortex beams and transformation optics, Journal of Optics 21 (6) (2019) Article number 065401, doi: 10.1088/2040-8986/ab1743.
[20] A. A. Quarta, G. Mengali, Solar sail capabilities to reach elliptic rectilinear orbits, Journal of Guidance, Control, and Dynamics 34 (3) (2011) 923–926, doi: 10.2514/1.51638.
[21] A. A. Quarta, G. Mengali, Optimal solar sail transfer to linear trajectories, Acta Astronautica 82 (2) (2013) 189–196, doi: 10.1016/j.actaastro.2012.03.005.
[22] M. Bassetto, L. Niccolai, A. A. Quarta, G. Mengali, Logarithmic spiral trajectories generated by solar sails, Celestial Mechanics and Dynamical Astronomy 130 (2) (2018) Article number 18, doi: 10.1007/s10569-017-9812-6.
[23] G. Mengali, A. A. Quarta, D. Romagnoli, C. Circi, H^2-reversal trajectory: A new mission application for high-performance solar sails, Advances in Space Research 48 (11) (2011) 1763–1777, doi: 10.1016/j.asr.2010.11.037.
[24] X. Zeng, G. Vulpetti, C. Circi, Solar sail H-reversal trajectory: A review of its advances and applications, Astrodynamics 3 (1) (2019) 1–15, doi: 10.1007/s42064-018-0032-y.
[25] E. Aspnes, T. D. Milster, K. Visscher, Optical force model based on sequential ray tracing, Applied Optics 48 (9) (2009) 1642–1650, doi: 10.1364/AO.48.001642.
[26] D. Ma, J. Murray, J. N. Munday, Controllable propulsion by light: Steering a solar sail via tunable radiation pressure, Advanced Optical Materials 5 (4) (2017) Article number 1600668, doi: 10.1002/adom.201600668.
[27] J. Sauer, C. G., Optimum solar-sail interplanetary trajectories, in: AIAA/AAS Astrodynamics Conference, San Diego (CA), USA, 1976, AIAA Paper 76-792.
[28] G. Mengali, A. A. Quarta, Optimal three-dimensional interplanetary rendezvous using non-ideal solar sail, Journal of Guidance, Control, and Dynamics 28 (1) (2005) 173–177, doi: 10.2514/1.8325.
[29] L. Niccolai, A. A. Quarta, G. Mengali, Analytical solution of the optimal steering law for non-ideal solar sail, Aerospace Science and Technology 62 (2017) 11–18, doi: 10.1016/j.ast.2016.11.031.
[30] G. Mengali, A. A. Quarta, Near-optimal solar-sail orbit-raising from low earth orbit, Journal of Spacecraft and Rockets 42 (5) (2005) 954–958, doi: 10.2514/1.14184.
[31] M. Bassetto, A. A. Quarta, G. Mengali, Locally-optimal electric sail transfer, Proceedings of the Institution of Mechanical Engineers, Part G: Journal of Aerospace Engineering 233 (1) (2019) 166–179, doi: 10.1177/0954410017728975.
[32] A. E. Bryson, Y. C. Ho, Applied Optimal Control, Hemisphere Publishing Corporation, 1975, Ch. 2, pp. 71–87, ISBN: 978-0891162285.
[33] D. F. Lawden, Optimal Trajectories for Space Navigation, Butterworths & Co., London, 1963, pp. 54–60.